Applied Materials Today 26 (2022) 101268

Contents lists available at ScienceDirect

Applied Materials Today

journal homepage: www.elsevier.com/locate/apmt

Bamboo-inspired, simulation-guided design and 3D printing of light-weight and high-strength mechanical metamaterials

Zhi Zhang[1], Lei Zhang[1], Bo Song*, Yonggang Yao, Yusheng Shi

State Key Laboratory of Material Processing and Die and Mould Technology, School of Materials Science and Engineering, Huazhong University of Science and Technology, Wuhan 430074, China

ARTICLE INFO

Article history:
Received 18 August 2021
Revised 28 October 2021
Accepted 7 November 2021

ABSTRACT

Mechanical metamaterials, consisted of periodic arrangements of struts, exhibit excellent specific mechanical properties (kN•m/kg) and are of importance for aerospace applications, lightweight construction, bone implants, and energy absorption. However, current mechanical metamaterials are still falling far behind many biological architectures. On the other hand, biological materials often lack design flexibility and controllable structures, and mechanical performances. Here, inspired by the strong and ductile bamboo with a hollow architecture, we constructed three face-centered cubic (FCC) lattice-based mechanical metamaterials via selective laser melting of Ti-6Al-4 V with high fidelity. Guided by the numerical simulation, these biomimetic structures can be easily tailored through tuning the outer and inner (hollow) diameters with widely adjustable performances, resulting in a high compressive specific strength (87.19 kN•m/kg) at a low density (1.25 g/cm^3) without losing isotropy in the octet-truss configuration (d_i=0.59 mm, d_o=1.10 mm). Our study, therefore, provides a biomimetic strategy to realize simultaneously light-weight and high-strength mechanical metamaterials with a hollow topology.

1. Introduction

Despite recent advances in the design and fabrication of lightweight architectures, the ability to create parts that possess both lightweight, high strength, and isotropy remains a challenge as these properties are often mutually restricted [1,2]. Mechanical metamaterials composed of a periodic or aperiodic arrangement of unit cells have the characteristics of light-weight, high specific strength, and high energy absorption as well as peculiar mechanical performances, thereby which were widely used in the aerospace industry, biomedical field, vehicle engineering [3–6]. Their magnitude of relative density, geometrical size of a unit cell, and distribution of multiple microstructures could be engineered for specific mechanical performances. Particularly, lattice-based mechanical metamaterials inspired by the “atom-to-atom” connection with strong designability and controllable mechanical performances receive extensive research and attention [7–9]. Nevertheless, due to the limits of traditional processing methods, mechanical metamaterials with intricate topologies could not be available, resulting in the research remain theoretical expression.

In recent years, mechanical metamaterials have been regaining a remarkably increasing interest, owing to the rapid development of additive manufacturing (AM)/3D printing [10–13]. Powder bed fusion (PBF) can directly form computer-aided design (CAD) models by the interaction of laser and powder models [14]. Selective laser melting (SLM) and electron beam melting (EBM) are the representative PBF processes to manufacture metal parts with high-precision geometrical characteristics, thus acting as an ideal tool for manufacturing mechanical metamaterials with a complex design [15–17]. For example, Ataee et al. designed and fabricated ultrahigh-strength Ti-6Al-4 V gyroid lattice metamaterials via SLM, which possessed the specific strength of 36.65 kN•m/kg with 0.82 porosity [18]. However, lattice topological mechanical metamaterials were still largely limited to inefficient strut-geometries, and importantly, are still fall further behind many biological architecture materials with a unique structure.

After millions of years of evolution and development, natural materials have formed excellent macro-/micro-structures occurred in nature or human system which supports specific functions and exhibited particular properties. For instance, the Pantheon dome-like architected metamaterials with a gradient helix could withstand high load while being low density [19]. The whale baleen exhibited excellent mechanical strength as well as superior toughness due to the ordered microstructures [20]. The natural bamboo had characteristics of lightweight and high strength for its special

* Corresponding author.
E-mail address: bosong@hust.edu.cn (B. Song).
[1] These authors contributed equally to this work.

https://doi.org/10.1016/j.apmt.2021.101268
2352-9407/

macro and micro hollow structure, which possessed a strength of 352.57 MPa and far stronger than other natural materials [21]. The hollow structures inspired by bamboo currently possessed distinct light-weight levels, specific strengths, and energy absorption performances [22]. However, simple biological architecture materials were lack of controllable complexity, designability, and mechanical performance. Besides, nature-inspired structures tended to be superior in one direction only and showed evident anisotropy. The problem of anisotropy could be well solved by the combination of different lattice metamaterials [23], but different featured sizes in the same structure topology would increase the difficulty of structure design. Therefore, it was challenging to obtain simultaneously light-weight, high-strength, and isotropic properties which would require suitable materials and delicate structure design. Our published review paper shown that mechanical metamaterials with controllable geometric topology and physical properties could be realized by using the idea of structural feature combination [24].

In this work, inspired by atom packing and bamboos' morphologies, a combinatorial biomimetic strategy to realize lattice-based mechanical metamaterials, i.e. FCC, octahedron, and octet-truss, with simultaneous light-weight, high-strength and isotropic properties were proposed. The bio-inspired lattice-based mechanical metamaterials (BLMMs) with excellent performance were obtained by simulation-guided design and fabricated by SLM. The manufacturability, mechanical responses, and stress distributions of optimized mechanical metamaterials were investigated via micro-CT, compression experiments, and finite element method, respectively. The underlying mechanisms of the bamboo-like effect on the mechanical properties and stress distributions were further discussed.

2. Materials and methods

2.1. Materials and SLM process

The raw materials of a gas-atomized Ti-6Al-4V powder for SLM were used in this work. The Ti-6Al-4V powder had the following geometrical properties of particles: D_{10}: 20.0 μm, D_{50}: 32.2 μm, D_{90}: 49.6 μm. The BLMMs, i.e. FCC, octahedron, and octet-truss, were fabricated via an M290 type SLM equipment (EOS, Germany). The optimized SLM processing parameters were determined as a laser power of 280 W, a scanning speed of 1200 mm/s, a layer thickness of 30 μm, a hatch distance of 140 μm, and scanning direction rotated by 67 ° alternately between adjacent layers. The SLM-completed BLMM samples were obtained by using wire-cut electrical discharge machining (wire-EDM). Then, adhesive powder particles on the SLM-fabricated BLMMs, i.e. FCC, octahedron, and octet-truss, were removed by ultrasonic cleaning in pure ethyl alcohol and thereby shot blasting, in turn.

2.2. Morphological characterization and mechanical tests

The Ti-6Al-4V particle's diameter distribution was tested by using Mastersizer 3000 laser diffraction particle size analyzer (Malvern Panalytical Inc., UK). The SLM additive manufacturability of optimized lattice-based mechanical metamaterials was quantitatively analyzed by SkyScan 1176 X-ray computed tomography (CT) (Bruker, Germany). The filter used for scanning Ti-6Al-4V samples was Al + Cu. The reconstructed micro-CT data set had an isotropic voxel size of 18.0 µm. These data were further analyzed and visualized by using commercially available image analysis software VG Studio Max 3.0 (Volume Graphics GmbH, Heidelberg, Germany). EPMA-8050 G scanning electron microscope (SEM) (Shimadzu, Japan) was utilized to analyze the surface morphology of the SLM-built lattices. Uniaxial quasi-static compression tests were carried out at a loading rate of 1.2 mm/min using an AG-IC100 KN Electronic Universal Testing Machine (Shimadzu, Japan) at room temperature. Meanwhile, a digital camera was used to capture track of observation on the whole deformation process. To have a better understanding of the mechanical responses, Young's modulus and compressive yield strength were determined from the stress-strain line graphs following ISO 13,314:2011. The energy absorption capacity of cellular structures was determined using numerical integration from 0 to onset strain of densification, calculating the area under the stress-strain curves.

2.3. Modeling approach of compression mechanics

2.3.1. Representative volume element model

For periodic BLMMs, To investigate the effect of bamboo-like level and outer diameter size on the elastic properties of BLMMs, an ideal representative volume element model composed of a unit cell was adopted. The periodic boundary condition was implemented by setting the equal strain on the different opposite surfaces [25,26]. The void volume fraction, which was the difference of unit space volume and BLMMs's volume, the representative volume element model exacted from CAD software was determined. The homogenization theory was used to derive the elastic matrix [27]. The free tetrahedron mesh element was set as 0.15 mm, shown in Fig. S6. Thus, total mesh size ranged from around 64,000 to 86,000 elements for FCC, octahedron, and octet-truss bamboo-like lattice models, respectively, when the mesh sizes of around 50,000 elements per unit cell were sufficient to reduce the simulated discretization errors to marginal level [28]. Due to the cubic symmetry of the BLMM structural designs, the elastic tensor contained only three independent components (i.e., C_{11}, $C_{12,}$ and C_{44}). The equivalent Young's modulus in [100] direction and the Zener anisotropy index for cubic crystals could be calculated using the following Equations [26].

$$E^* = \frac{{C_{11}}^2 + C_{11}C_{12} - 2{C_{12}}^2}{C_{11} + C_{12}} \tag{1}$$

$$\xi = \frac{2C_{44}}{C_{11} - C_{12}} \tag{2}$$

To compare the normalized Young's modulus between bamboo-like BLMMs and HS bound, the Hashin–Shtrikman (HS) bound and the difference of normalized Young's modulus was determined as [1]:

$$\frac{E_{HS}}{E_s} = \frac{2\overline{\rho}(5\nu - 7)}{13\overline{\rho} + 12\nu - 2\overline{\rho}\nu - 15\overline{\rho}\nu^2 + 15\nu^2 - 27} \tag{3}$$

$$\Delta E^* = E_{HS} - E^* \tag{4}$$

where ρ was the relative density, ν was the Poisson's ratio, and E_s was Young's modulus of the Ti-6Al-4V material.

2.3.2. Quasi-static compression simulation

To capture the stress distribution and visualizing deformation, the nonlinear finite-element (FE) quasi-static compression simulation was conducted by commercial software COMSOL multiphysics. Material properties of SLM-fabricated Ti-6Al-4V for the FE method were shown in Fig. S7. The BLMMs were sandwiched between two rigid flat plates, which simulated the experimental compression conditions. The top plate only was allowed to move along the Z-axis while the bottom plate was fixed in all directions. The frictional coefficient regarded as static friction between plates and samples was set as 0.15. A free tetrahedron element was used to mesh the model. SLM-built parts were believed to have potential metallurgical defects and manufacturing deviations compared to designed ones [2,26]. Some assumptions were made in this FE method to simplify the simulated model. The first assumption is

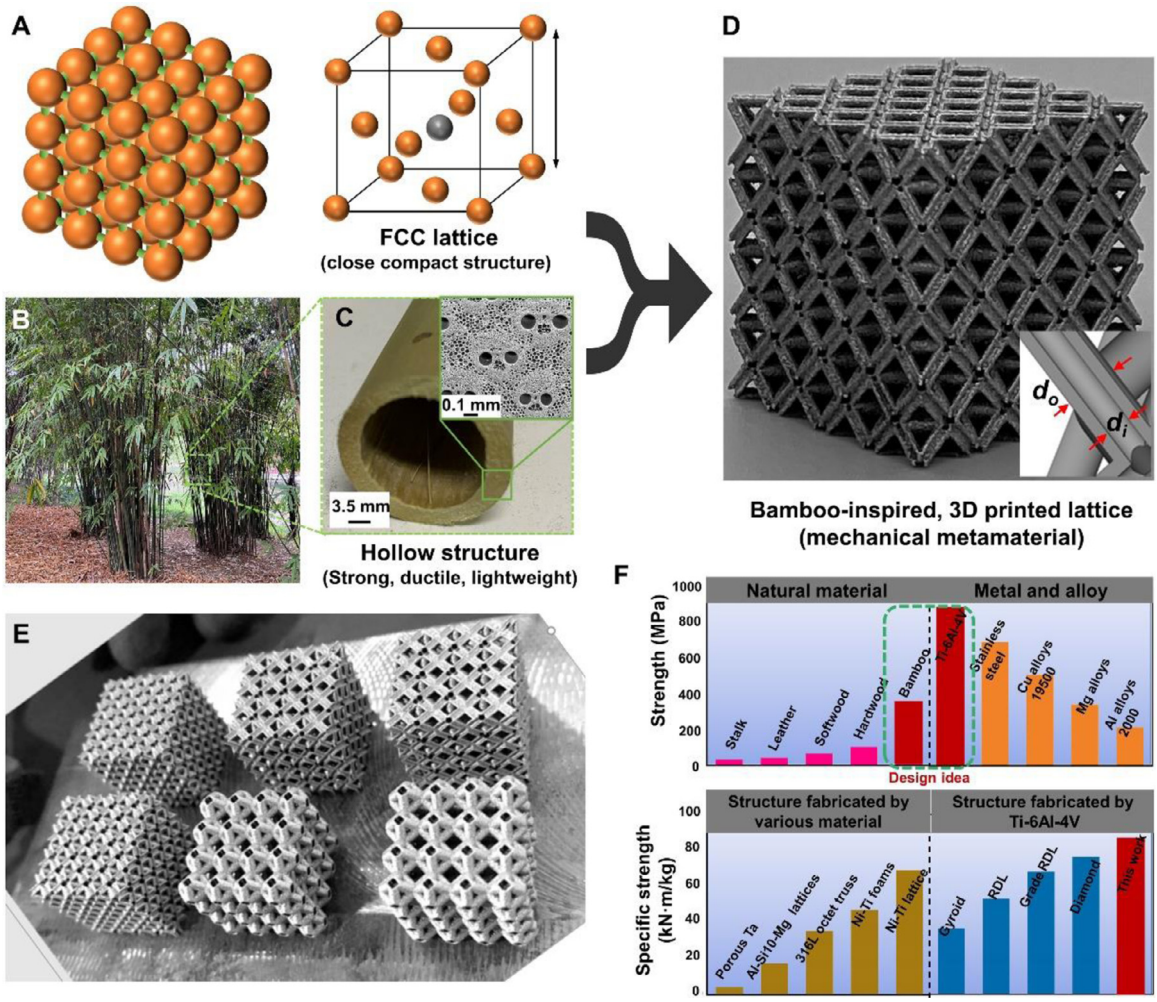

Fig. 1. Lattice-based mechanical metamaterials inspired by atoms' packing and bamboo's hollow features. (A) The micro-morphology of lattice atoms. (B-C) The macro- and micro- morphological characteristics of bamboos. (D) Bio-inspired octet-truss mechanical metamaterials with outer diameter, do, and inner diameter, di. (E) SLM-printed three lattice constructions of FCC, octahedron, and octet-truss. (F) The strength of typical biomaterials as well as the specific strength of metals and various topological structures [17,18,21,30–35].

that the SLM-made BLMM structures are consistent with the as-designed CAD models. The second assumption is that the whole material property of the SLM-built BLMM specimens is still the same as the materials tested through standard tensile samples.

3. Results and discussion

3.1. Design principle

Normally, mechanical metamaterial are obtained by periodic or aperiodic arrangements of lattices, inspired by crystallographic atoms, in which lattices can be produced by connecting atoms through the strut, plate, and shell [2,5,29]. Compared to plate- and shell-based microlattices, strut-based lattices are capable of geometrical spatial transformation to cater to different design requirements. However, the low stiffness of strut-based lattices is one of the reasons for its narrow application range. Natural bamboos with high specific strength have strongly attracted our attention. After observing the macro and micro structures of bamboo, the multi-level hollow structure of bamboos is the key to its light weight and high strength. Therefore, inspired by atom packing and bamboos' morphologies, a combinatorial biomimetic strategy to realize lattice-based mechanical metamaterials with simultaneous light-weight, high-strength and isotropic properties were proposed.

Fig. 1 showed morphological evolution of isotropic lattice-based mechanical metamaterials inspired by atoms' space distributions and bamboo's hollow features. Fig. 1A presented the micro-morphology of lattice atoms. The lattice is a close compact structure arranged by atoms and the space distribution affects the properties. FCC and octet-truss lattices had the same spatial distribution of atoms. Fig. 1B-C showed the macro- and micro- morphological characteristics of natural bamboos, in which the through-hole structure made it behave with noteworthy mechanical strength. Besides, the macro- and micro- hierarchical structure contained the apparent hollow pores and microscopic void features, resulting in better structural rigidity and energy-absorption capacity of bamboos comparable with other plants (Fig. S1). Combining lattice atoms with bamboo hollow structures, bio-inspired octet-truss mechanical metamaterials with outer diameter, d_o, and inner diameter, d_i were available, shown in Fig. 1D. Considering the morphology of periodic BLMMs, the strut-based solid part and void space constructed a complete unit cell, in which the void space could be regarded as apparent pores in bamboos. Then, through introducing the bamboo-like levels (d_i/d_o), the second microstructure was embedded into traditional lattice structures, which was equivalent to the microscopic void features in bamboos. Thus, the lattice structural design and bamboo-like strut together constituted BLMMs, which can further affect the density, mechanical properties, as well as isotropy of BLMMs.

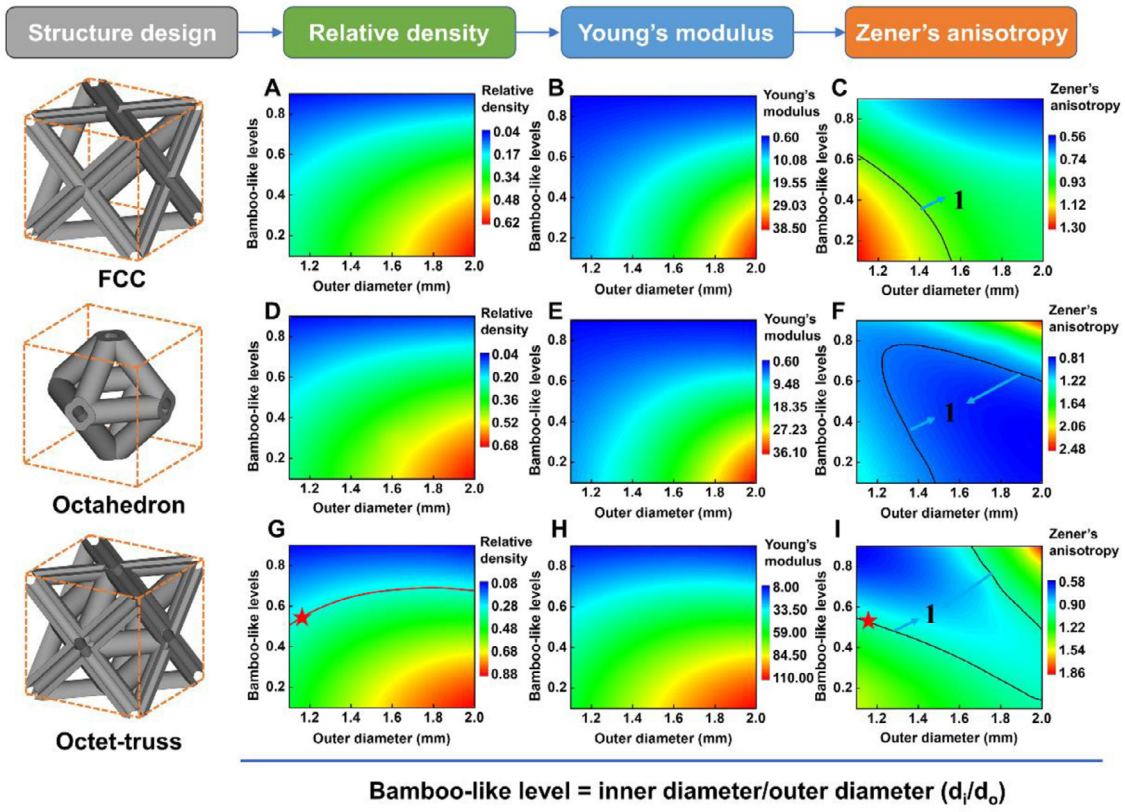

Fig. 2. Numerical physical properties of FCC, octahedron, and octet-truss bio-inspired lattice-based mechanical metamaterials. (A, D, G) Relative density, (B, E, H) Young's modulus, and (C, F, I) Zener's anisotropy as a function of the bamboo-like level and the outer diameter.

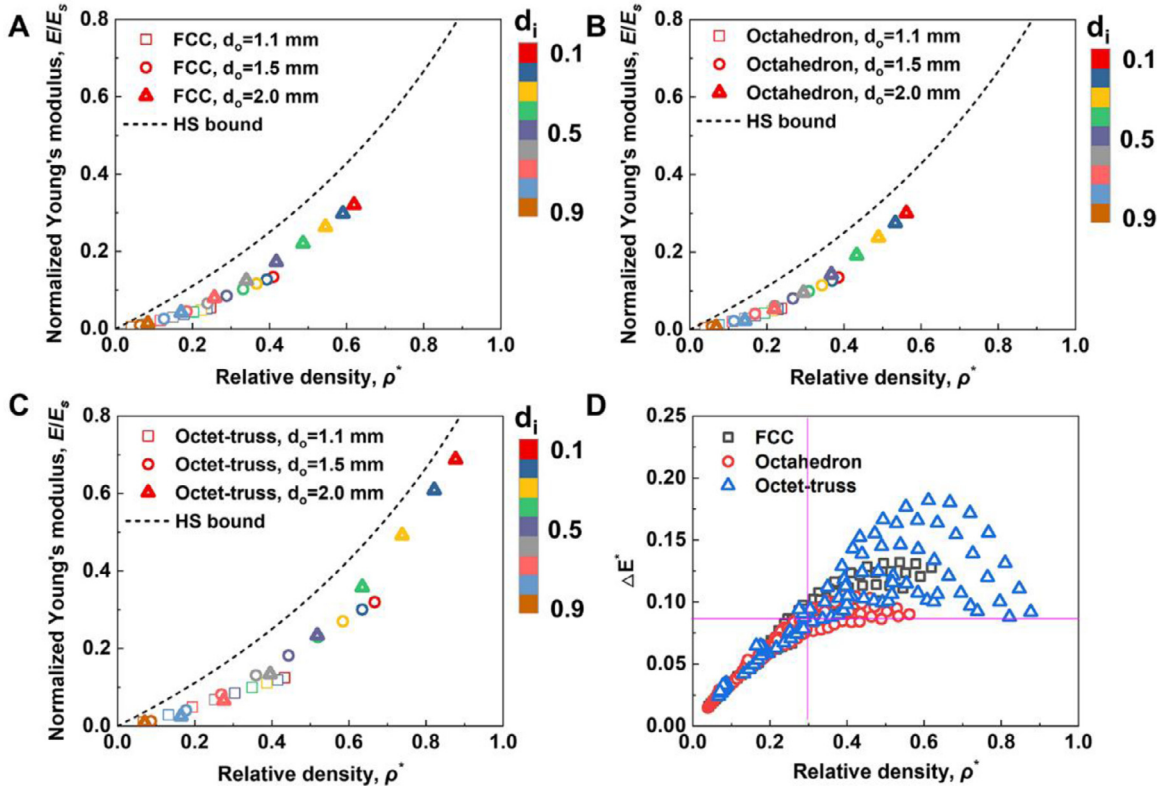

Fig. 3. The relationship between normalized Young's modulus and relative density of (A) FCC, (B) octahedron, and (C) octet-truss bio-inspired lattice-based mechanical metamaterials. (D) The difference comparison of normalized Young's modulus of bio-inspired lattice-based mechanical metamaterials and HS bound.

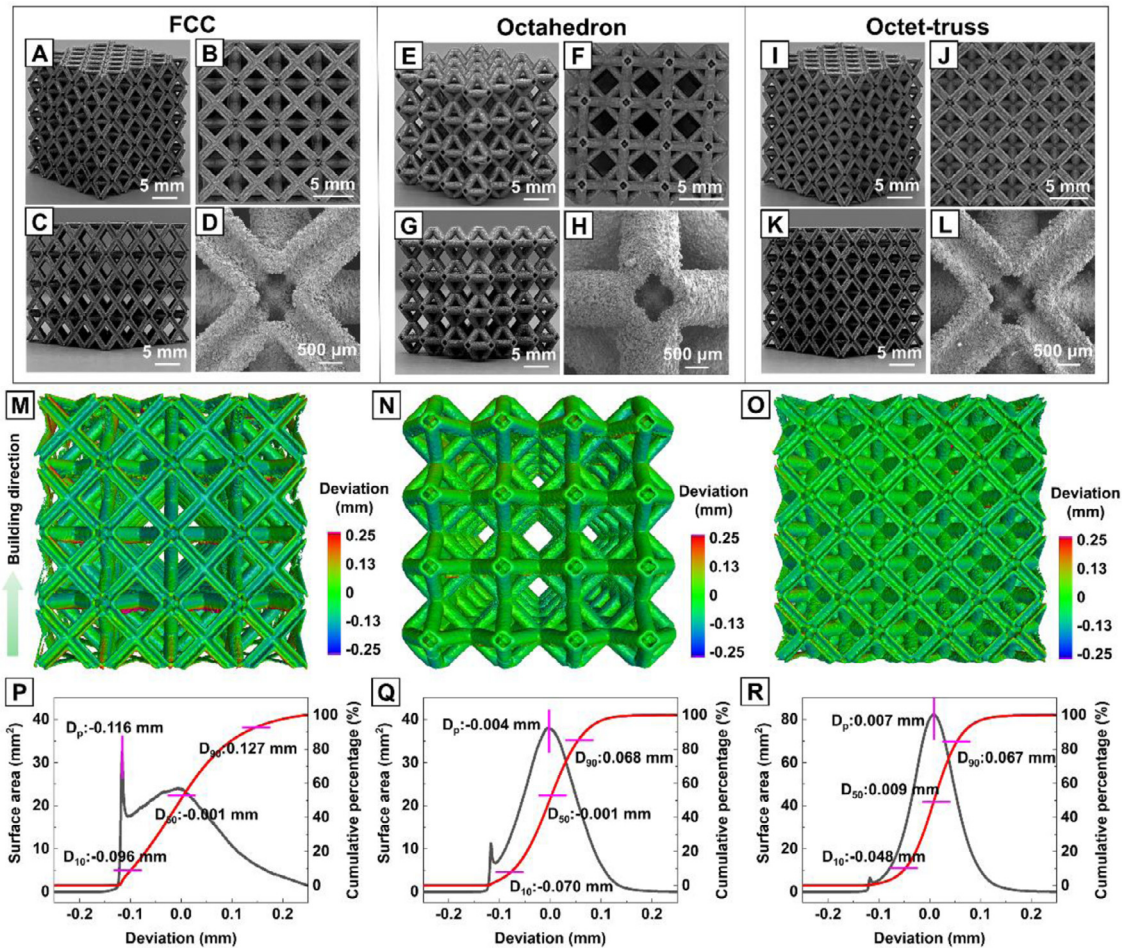

Fig. 4. Ti-6Al-4 V metallic specimens of 28.9% relative density fabricated through SLM. (A-D) FCC bamboo-like BLMMs specimens: A. [111] view, B. [010] view, C. [110] view, D. SEM lateral view. (E-H) Octahedron bamboo-like BLMMs specimens: E. [111] view, F. [010] view, G. [110] view, H. SEM lateral view. (I-L) Octet-truss bamboo-like BLMM specimens: I. [111] view, J. [010] view, K. [110] view, L. SEM lateral view. (M-O) Three-dimensional surface deviation maps of X-ray CT data analysis and (P-R) statistical surface deviation distributions for FCC, octahedron, and octet-truss bamboo-like BLMMs specimens, respectively. (Dp was the peak surface deviation, *d*-values (D10, D50, and D90) indicated the intercepts for 10, 50, and 90% of the cumulative percentage.)

Guided by numerical simulation, the FCC, octahedron, and octet-truss BLMMs with outer diameter (d_o =1.10 mm) and inner diameter (d_i =0.59 mm) were obtained by 3D SLM printing of Ti-6Al-4V (Fig. 1E), showing a low density of 0.74, 0.70, and 1.25 g/cm^3. The unit cell length of BLMMs was all 5 mm and the overall dimensions were 20 × 20 × 20 mm^3. Our BLMM combines the unique structure advantage of bamboo (strong and ductile) and the high strength of Ti-alloy (Fig. 1F above), thus achieving a record-high specific strength up to 87.19 kN•m/kg, more than most materials and structure designs among current literature [17,18,21,30–35](Fig. 1F). The current structural design and material construction can open up a biomimetic strategy to realize lightweight and high-strength mechanical metamaterials with a hollow topology.

3.2. Numerical optimization

To obtain simultaneously lightweight, high strength, and isotropic mechanical metamaterials, numerical simulation was performed to guide the structural design using the representative volume element method. We explored both (1) different atom structure designs (FCC, octahedron, and octet-truss BLMMs) and (2) parameters mapping of bamboo-like struts (different bamboo-like levels, d_i/d_o and outer diameters, d_o). Fig. 2 presented simulated physical properties of FCC, octahedron, and octet-truss BLMMs. The relative density of FCC, octahedron, and octet-truss BLMMs both increased with the increase of the outer diameter and the decrease of the bamboo-like level (Fig. 2A, D, G). Analogously, Young's modulus of FCC, octahedron, and octet-truss BLMMs both went up with the rise of the outer diameter and the decline of the bamboo-like level (Fig. 2B, E, H). The variations of relative density and Young's modulus as a function of the bamboo-like level and the outer diameter were similar to each other because there was a Gibson-Ashby relationship between relative density and Young's modulus [36]. The Zener's anisotropy of these three BLMMs had distinct relationships with the bamboo-like level and the outer diameter, which were attributed to different lattice topologies (Fig. 2C, F, I). The Zener's anisotropy of FCC BLMMs was monotonous with the bamboo-like level and the outer diameter while Zener's anisotropy of octahedron and octet-truss BLMMs were lack of regularity. It showed that the simulation guide could well explore the properties of bio-inspired structures with different structures and bamboo-like levels, so as to help choose the appropriate property combinations in the huge structure design space.

Under the premise of isotropy and a relative density of less than 30%, the higher the strength of BLMMs, the better. We determined octet-truss BLMMs with 28.9% relative density and 1 Zener's anisotropy level as an optimal solution, indicated by the red star point. This optimized octet-truss BLMM also behaved high-strength, which would be elaborated in the followed section. When

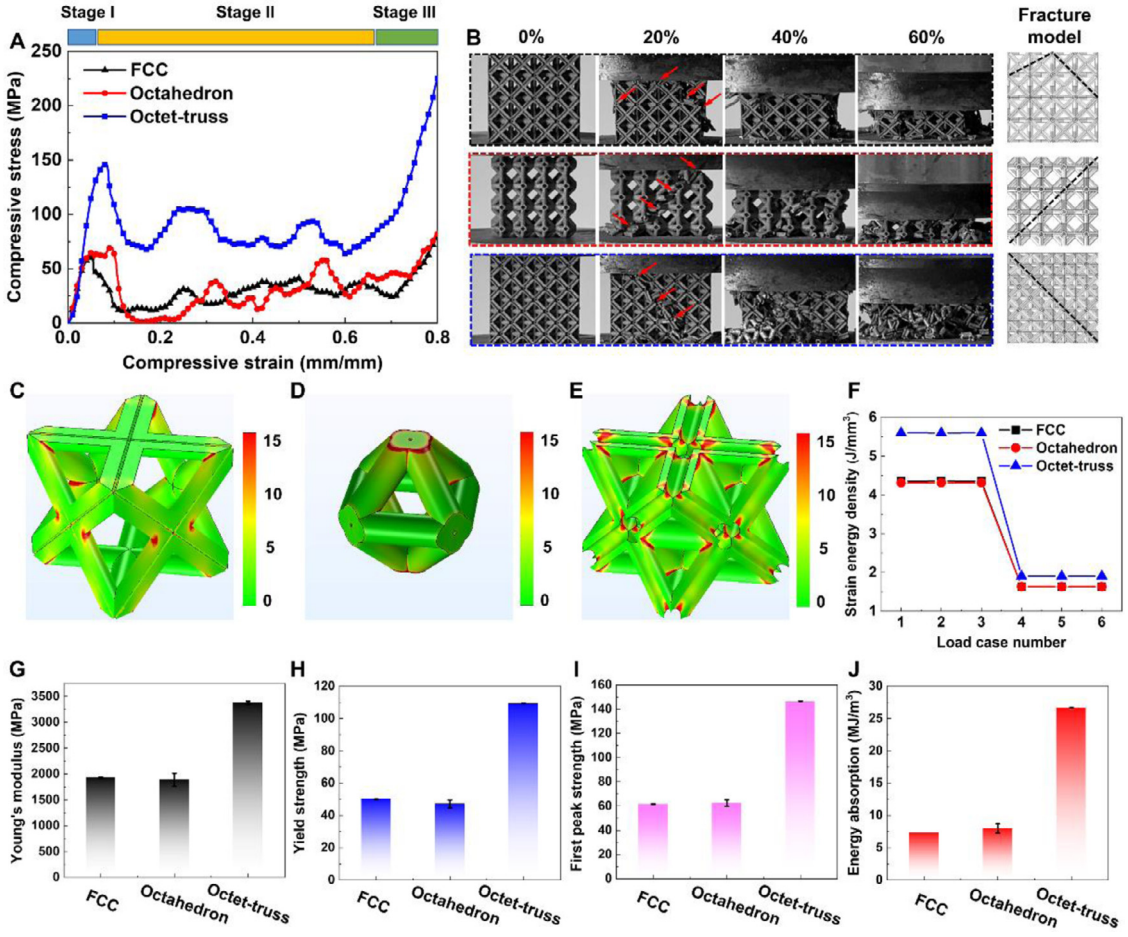

Fig. 5. Experimental mechanical response, deformation processes and simulated strain energy density of SLM-manufactured FCC, octahedron, and octet-truss bamboo-like BLMM specimens. (A) Stress-strain curves. (B) deformation processes and fracture modes. (C-E) Distribution of the simulated strain energy density within FCC, Octahedron, and octet-truss bamboo-like BLMMs, respectively, subject to uniaxial compression along the vertical direction. (F) The strain energy density versus the load case number. Experimental results of (G) Young's modulus, (H) yield strength, (I) first peak strength, and (J) energy absorption.

under the same bamboo-like level, the different outer diameters also caused different mechanical responses.

By comparing the Hashin–Shtrikman (HS) bound and the strength of bionic lattice structures, the relative density range of the optimal structure strength was further determined. The normalized Young's modulus of these different BLMMs, defined as the ratio of the stiffness under uniaxial loading in the [100] direction to the materials' modulus, had different scalings according to a power law of relative density ρ, as expected from the well-noted Gibson-Ashby relationships [36]. For the same structural configuration, the larger the outer diameter was, the larger the exponential coefficient and constant coefficient of the fitting results were (Fig. 3A–C), which was attributed to the increased relative density. With the unvaried inner diameter, the improved outer diameter would result in an increased volume used to resist deformation, then aggrandized the strength of bamboo-like lattices. For the identical outer diameter, the octahedron BLMMs had stronger sensitivity of the relative density compared with the other two structures (Table. S1). The difference of normalized Young's modulus was defined as the difference between the Hashin–Shtrikman (HS) bound and the normalized Young's modulus of these different BLMMs.

The different distributions of normalized Young's modulus presented a parabolic relationship as a function of the relative density and incomplete axisymmetry with the 60% relative density line (Fig. 3D). It was shown that the high-strength BLMMs with under 30% relative density greatly closed to the HS bound. This further proved that the above isotropic optimal solution also had high strength mechanical properties. The relative density of bamboo-like BLMMs was controllable by the outer diameter and inner diameter together. As illustrated before, the outer diameter determined the macroscopic porosity and the corresponding strength of lattices while the inner diameter, i.e., the bamboo-like feature, achieved the microscopic voids to further regulate the lightweight level, causing the phenomenon that the large outer diameter had increased E-ρ scaling exponents. Different from the traditional lattice structures, the hollow bioinspired lattice structures with different outer/inner diameters had a wider space to obtain different mechanical properties.

3.3. Experimental verification and mechanism analysis

3.3.1. Morphological characterization of SLM-printed samples

To validate our mechanical property estimates experimentally, we used 3D printing of selective laser melting (SLM) to fabricate FCC, octahedron, and octet-truss bamboo-like BLMMs specimens with a cubic unit cell of 5 mm from Ti-6Al-4V particles (Fig. 4A-L). For octet-truss bamboo-like BLMMs, a relative density of 28.9% was obtained from the superposition of FCC and octahedron diameter parameters of 0.59 mm and 1.10 mm, indicating the relative density of 16.72% and 15.92%, respectively. Prior to investigating the mechanical responses, the SLM manufacturing fidelity of FCC, octahedron, and octet-truss bamboo-like BLMMs specimens was quantificationally evaluated by the X-ray CT method (Fig. 4M-R). The

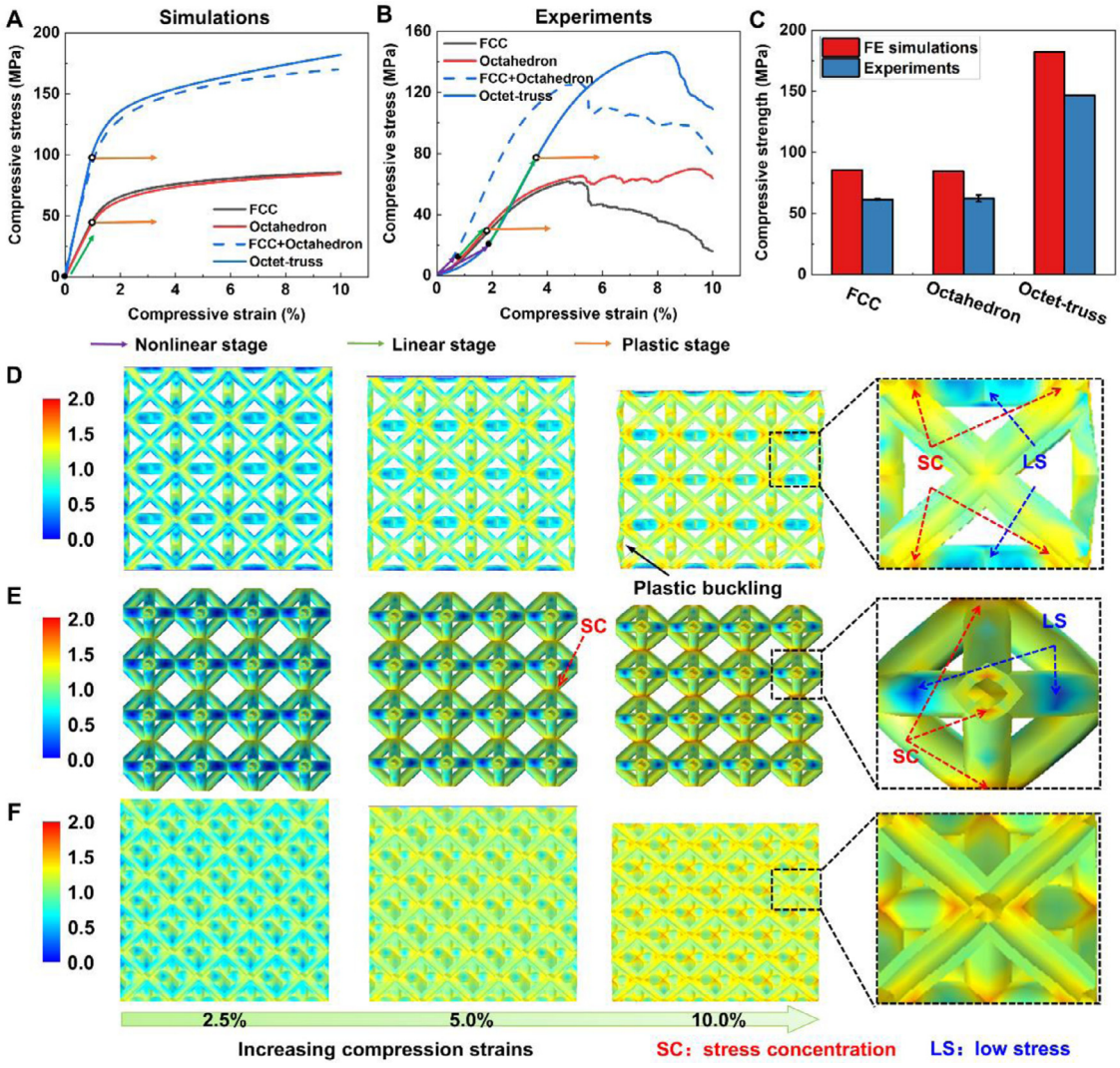

Fig. 6. Comparison of numerical and experimental mechanical responses of bamboo-like BLMM specimens. (A-B) Strain–stress curve and (C) compressive strength comparisons between simulations and experiments. (D-F) FE predicted stress distributions at different strains for FCC, octahedron, and octet-truss bamboo-like BLMMs specimens, respectively.

whole green color contour showed the surface deviation with rational acceptability (mostly below 0.25 mm). From the 3D surface deviation comparison, the manufacturing fidelity of FCC and octet-truss bamboo-like BLMMs specimens were the worst and the best, respectively (Figs. S2,S3). The maximum deviation that existed in the downward surfaces of horizontal struts indicated the red contour, which was due to the lack of support and the melted part with a larger weight comparable with raw particles on the powder bed. The D_{10}, D_{90} and D_p values of octet-truss bamboo-like BLMMs specimens were −0.048, 0.067, and 0.007 mm, superior to those of FCC (−0.096, 0.127, and −0.116 mm) and octahedron (−0.070, 0.068, and −0.004 mm) specimens. This was attributed to the that the decreased relative density of lattices would cause a larger molten pool to attract incompact particles onto the surface of molten solid parts. In contrast to octahedron bamboo-like BLMMs specimens with an approximate relative density, SLM-manufactured FCC lattices had larger manufacturing offset due to the overhanging topology. Sub-peak negative deviations were overtly presented in those specimens. This was contributed to the that the intricate bamboo-like features easily produced printing defects and overhanging struts increased the risk of dross and deformation. The outer surfaces of bamboo-like BLMMs and the upper surface of struts opposite to the location of dross defects would result in manufacturing difficulty and even collapse of the printed layer, then form negative deviations. Generally, the SLM forming BLMMs had good consistency with the original design ones and fine manufacturing fidelity. The manufacturing deviation is strongly related to the building process of metal AM and laed to the inconsistency of the parts due to its complexity. Recenlty, Sing et al., took the integration of machine learning into the different stages of L-PBF process chain, which potentially lead to better quality control [37]. Qin et al., proposed an automatic determination method of the part build orientation for laser powder bed fusion, in which the volumetric error, surface roughness, build time and build cost were evenly considered [38]. The further improvement of manufacturing fidelity could be realized by utilizing datasets obtained at various stages of the SLM process chain.

3.3.2. *Mechanical properties of SLM-printed samples*

Fig. 5 exhibited the experimental mechanical response, deformation processes and simulated strain energy density of SLM-manufactured FCC, octahedron, and octet-truss bamboo-like BLMMs specimens. All lattices experienced three typical deformation stages: elastic-plastic stage, stress oscillation stage, and densification stage (Fig. 5A). The FCC and octet-truss bamboo-like BLMM specimens with a close relative density showed a similar stress-

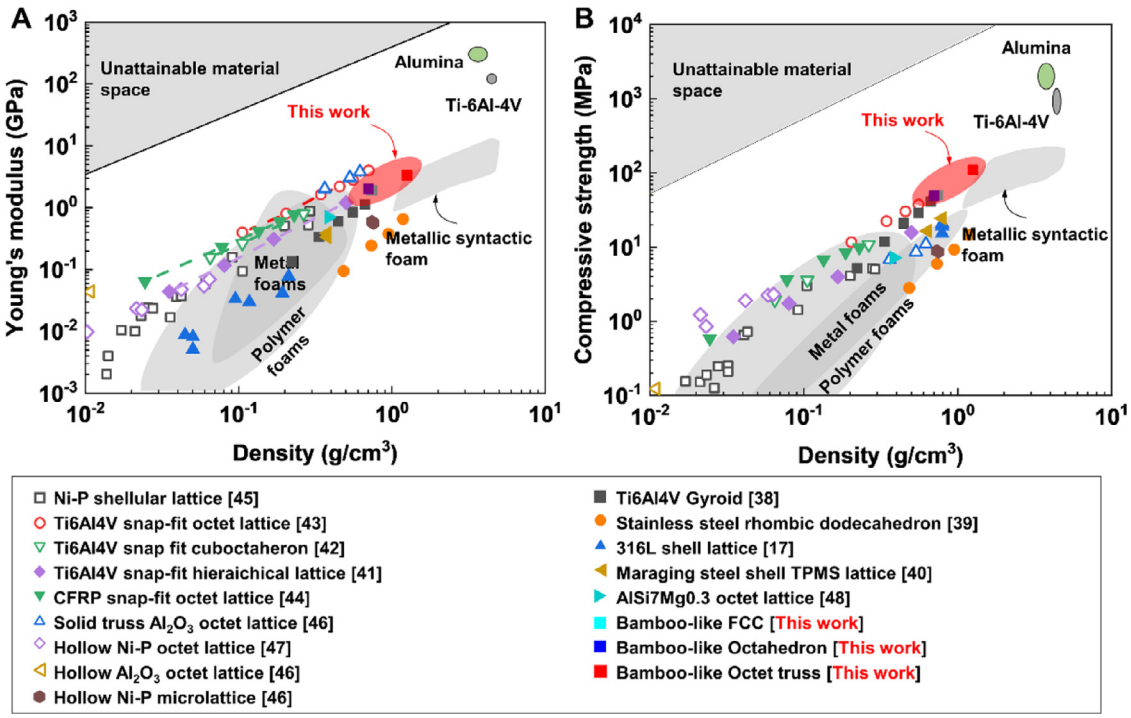

Fig. 7. Octet-truss bamboo-like BLMMs with excellent strength and moderate stiffness in existing lattice metamaterials for their corresponding density. (A) Young's modulus and (B) compressive strength Ashby property maps [17,39-47,49].

strain curve but displayed different deformation characteristics. The former showed the proximal layer destruction while the latter presented an inclined 45° fracture, which was ascribed to the different topologies (Fig. 5B). The octet-truss bamboo-like BLMM specimens also presented the inclined fracture model but along with a high-stress undulant platform to resist external loads.

We also performed the finite element simulation on these three BLMMs to understand their mechanical behaviors. As shown from the predicted spatial strain energy density distributions derived by the representative volume element model (Fig. 5C-E), the positions of connectivity nodes happened a concentration of strain energy density, which was corresponding to the observation of experimental sequential deformations that the connectivity nodes were earlier to break down through buckling than the inclined struts in all three structures. In different load cases, the octet-truss bamboo-like BLMM had the highest strain energy density due to more struts to disperse stress. The Young's modulus, yield strength of octet-truss bamboo-like BLMM specimens, 3.38 GPa and 109.52 MPa, were slightly lower or nearly equaled to sum of those of FCC, 1.93 GPa and 50.20 MPa, and octahedron specimens, 1.89 GPa and 49.55 MPa, respectively (Fig. 5G-J). The first peak strength and energy absorption of octet-truss bamboo-like BLMM specimens, 146.52 MPa and 26.65 MJ/m^3, were surpassed to sum of those of FCC, 61.08 MPa and 7.31 MJ/m^3, and octahedron specimens, 59.70 MPa, and 7.98 MJ/m^3. In the view of lightweight, strength, and isotropy, the octet-truss bamboo-like BLMM specimen had excellent comprehensive mechanical properties.

Given the elastic-plastic nature of the metallic constituent material, the plastic yield response could not be quantified from the liner-elastic simulation models. Instead, another series of compression mechanical simulations were conducted to study the yield strength of BLMMs using a rate-independent model. Fig. 6 presented the numerical mechanical responses and stress distribution of bamboo-like BLMM specimens. Due to the out of the flatness of specimens' top surfaces and experimental hard contact between specimens and metalheads, the nonlinear stage emerged in the elastic-plastic area, which caused the hysteresis of linear and plastic stages (Fig. 6A-B). The numerical compressive strength of these three bamboo-like BLMM specimens was 85.57, 84.61, and 182.18 MPa, which closed to the strength of 61.5, 62.46, and 146.53 MPa expected from experiments (Fig. 6C). The reasonable strength overestimation of numerical calculation was due to the inconsistency between the SLM manufacturing samples and the design samples in terms of geometry and material microstructure properties. From the Von Mises stress contours, the stress concentration was more evident with the increasing compression strains and predominantly distributed in connectivity nodes of struts while the horizontal struts always remained low-stress state (Fig. 6D-F). Essentially, the higher amounts of high-stress distribution in a lattice structure, the higher the strain energy needed for bending or stretching deformation of struts, therefore, the position of stress concentration was consistent with that of strain energy density concentration distributions. It was noted that the maximum von Mises stresses observed in the central BLMMs were evenly distributed nearby the wherein nodal points but formed localized high-stress bands along the diagonal line of the whole BLMMs. With the increase of compressive strains, plastic buckling of oblique struts was developed, leading to early plastic hinges formation in the junctions of peripheral BLMM cells. Besides, from the von Mises stress distributions plots in the BLMM cells, areas of stress concentration and low stress were uneven distribution within a lattice cell. For FCC lattices, the higher amounts of high-stress distribution in longitudinal struts than horizontal struts. Similarly, the stress was more concentrated in longitudinal struts than in horizontal struts for octahedron lattices. On the contrary, for octet-truss lattices, the stress was evenly distributed on the joints and struts, in which areas of low stress were not significantly presented, however, high-stress concentrations were observed on lattice nodes. This owed to the high strut to node ratio of the octet-truss lattices, for which the motion of nodes would be

inevitably limited by struts and the deformation was more strongly dependent on the bending/twisting of strut members than the FCC and octahedron lattices.

The analytical calculations of these bamboo-like BLMMs were completed to understand the underlying mechanism of mechanical responses shown in Figs. S4,S5. Pure contact force-acted inclined struts with the number of 8, 4, and 12 and 45 ° angle of slope consisted of the FCC, octahedron, and octet-truss bamboo-like BLMMs, respectively. It was noted that FCC and octahedron lattices had strut-node connectivity of $Z = 2$ and $Z = 8$, as well as Maxwell number of $M = 12$ and $M = 0$, respectively, therefore, were bending-dominated and stretching-dominated lattice topologies, respectively. With high nodal connectivity of $Z = 12$ and Maxwell number of $M = 0$, octet-truss lattices provided a solution for high-strength stretching dominated topology, further with glorious energy absorption capacity derived by the bamboo-like feature.

3.3.3. Comparison with other lattice metamaterials

Fig. 7 displayed Young's modulus and compressive strength Ashby property maps comparing to various existing lattice metamaterials. The octet-truss bamboo-like BLMMs with excellent strength and moderate stiffness surpassed most lattice or porous metallic foam architectures. The stiffness and strength of SLM-built bamboo-like BLMMs were superior to SLM-manufactured Gyroid [39], rhombic dodecahedron [40], TPMS shell lattices [41], but only weak on the stiffness and equal on the strength to snap-fit lattices [42–45], which was due to their flawless materials and reinforced nodes, however, the lengthy manufacturing process limited mass production. The specific stiffness and strength of novel shellular lattices [46] and hollow lattices [47,48] were comparable to our SLM-built bamboo-like BLMMs. The strength of our SLM-built octet-truss bamboo-like BLMMs also significantly preceded homogenous solid truss Al_2O_3 and Al-based octet lattices [47,49].

4. Conclusion

Inspired by geometrical morphologies of the atom and the bamboo, we proposed a combinatorial biomimetic strategy to realize bio-inspired lattice-based mechanical metamaterials with hollow struts and simultaneous light-weight, high-strength, and isotropic properties. Guided by numerical simulation, we explored different structure designs as well as bamboo-like levels and obtained optimized performances in an octet-truss design (d_i=0.59 mm, d_o=1.10 mm). The additively SLM-manufactured BLMMs show high manufacturing fidelity with a superior specific strength (87.19 kN•m/kg) at a low density (1.25 g/cm^3), benefited by our combinatorial biomimetic strategy. The comparison of stiffness and strength confirmed that the proposed BLMM architectures remained stiffer and stronger than most lattice or porous metallic foam architectures. This work provided a train of thought for conceiving high-performing engineering architectures through the way of multiple bionic strategies.

Declaration of Competing Interest

We declare that we have no financial and personal relationships with other people or organizations that can inappropriately influence our work, there is no professional or other personal interest of any nature or kind in any product, service and/or company that could be construed as influencing the position presented in, or the review of, the manuscript entitled, "Bamboo-inspired, simulation-guided design and 3D printing of light-weight and high-strength mechanical metamaterials".

CRediT authorship contribution statement

Zhi Zhang: Conceptualization, Investigation, Methodology, Data curation, Formal analysis, Visualization, Writing – original draft. **Lei Zhang:** Conceptualization, Investigation, Methodology, Data curation, Formal analysis, Visualization, Writing – original draft. **Bo Song:** Conceptualization, Writing – review & editing, Supervision. **Yonggang Yao:** Writing – review & editing. **Yusheng Shi:** Writing – review & editing.

Acknowledgments

Zhi Zhang and Lei Zhang contributed equally to this work. This work was sponsored by the Natural and Science Foundation of China (Grant No. 51922044, 51775208), the Key-Area Research and Development Program of Guangdong Province (No. 2020B090923001), the Academic frontier youth team (2018QYTD04) at Huazhong University of Science and Technology (HUST). The authors thank the Analytical and Testing Center of HUST for SEM examination and the State Key Laboratory of Materials Processing and Die & Mould Technology for test and compression tests.

Supplementary materials

Supplementary material associated with this article can be found, in the online version, at doi:10.1016/j.apmt.2021.101268.

References

[1] C. Crook, et al., Plate-nanolattices at the theoretical limit of stiffness and strength, Nat. Commun. 11 (1) (2020) 1579.
[2] L. Zhang, et al., Topology-optimized lattice structures with simultaneously high stiffness and light weight fabricated by selective laser melting: Design, manufacturing and characterization, J. Manuf. Process. 56 (2020) 1166.
[3] B. Deng, et al., Composite bending-dominated hollow nanolattices: A stiff, cyclable mechanical metamaterial, Mater. Today 21 (5) (2018) 467.
[4] T. van Manen, et al., Kirigami-enabled self-folding origami, Mater. Today 32 (2020) 59.
[5] A. Alomarah, et al., Compressive properties of 3D printed auxetic structures: experimental and numerical studies, Virtual Phys. Prototyp. 15 (1) (2019) 1.
[6] J. Mueller, et al., Stiffness-Independent Toughening of Beams through Coaxial Interfaces, Adv. Sci. 5 (11) (2018) 1800728 (Weinh).
[7] Y. Li, et al., Additively manufactured biodegradable porous iron, Acta Biomater. 77 (2018) 380.
[8] S. Xu, et al., Design of lattice structures with controlled anisotropy, Mater. Des. 93 (2016) 443.
[9] S.J. Yeo, et al., Structurally Controlled Cellular Architectures for High-Performance Ultra-Lightweight Materials, Adv. Mater. 31 (34) (2019) e1803670.
[10] B. Jenett, et al., Discretely assembled mechanical metamaterials, Sci. Adv. 6 (2020) eabc9943.
[11] S. Shan, et al., Multistable Architected Materials for Trapping Elastic Strain Energy, Adv. Mater. 27 (29) (2015) 4296.
[12] W. Yang, et al., Acoustic absorptions of multifunctional polymeric cellular structures based on triply periodic minimal surfaces fabricated by stereolithography, Virtual Phys. Prototyp. 15 (2) (2020) 242.
[13] K. Tang, et al., 3D printed hybrid-dimensional electrodes for flexible micro-supercapacitors with superior electrochemical behaviours, Virtual Phys. Prototyp. 15 (sup1) (2020) 511.
[14] S.L. Sing, W.Y. Yeong, Laser powder bed fusion for metal additive manufacturing: perspectives on recent developments, Virtual Phys. Prototyp. 15 (3) (2020) 359.
[15] D. Shamvedi, et al., 3D Metal printed heat sinks with longitudinally varying lattice structure sizes using direct metal laser sintering, Virtual Phys. Prototyp. 13 (4) (2018) 301.
[16] S.Y. Choy, et al., Superior energy absorption of continuously graded microlattices by electron beam additive manufacturing, Virtual Phys. Prototyp. 16 (1) (2021) 14.
[17] T.D. Thomas, et al., Additively-manufactured metallic micro-lattice materials for high specific energy absorption under static and dynamic loading, Acta Mater. 116 (2016) 14.
[18] A. Ataee, et al., Anisotropic Ti-6Al-4V gyroid scaffolds manufactured by electron beam melting (EBM) for bone implant applications, Mater. Des. 137 (2018) 345.
[19] L. Cheng, et al., The Twisting of Dome-Like Metamaterial from Brittle to Ductile, Adv. Sci. 8 (2021) 2002701.
[20] B. Wang, et al., Lessons from the Ocean: Whale Baleen Fracture Resistance, Adv. Mater. 31 (3) (2019) e1804574.

[21] Z. Li, et al., A Strong, Tough, and Scalable Structural Material from Fast-Growing Bamboo, Adv. Mater. 32 (10) (2020) e1906308.
[22] M. Zou, et al., A bionic method for the crashworthiness design of thin-walled structures inspired by bamboo, Thin-Walled Struct. 101 (2016) 222.
[23] T. Tancogne-Dejean, D. Mohr, Elastically-isotropic truss lattice materials of reduced plastic anisotropy, Int. J. Solids Struct. 138 (2018) 24.
[24] J. Fan, et al., A review of additive manufacturing of metamaterials and developing trends, Mater. Today (2021). In press.
[25] X.Y. Zhang, et al., Topological design, permeability and mechanical behavior of additively manufactured functionally graded porous metallic biomaterials, Acta Biomater. 84 (2019) 437.
[26] L. Zhang, et al., A topology strategy to reduce stress shielding of additively manufactured porous metallic biomaterials, Int. J. Mech. Sci. 197 (2021) 106331.
[27] D. Melancon, et al., Mechanical characterization of structurally porous biomaterials built via additive manufacturing: experiments, predictive models, and design maps for load-bearing bone replacement implants, Acta Biomater. 63 (2017) 350.
[28] I. Maskery, et al., Effective design and simulation of surface-based lattice structures featuring volume fraction and cell type grading, Mater. Des. 155 (2018) 220.
[29] A. Ataee, et al., Ultrahigh-strength titanium gyroid scaffolds manufactured by selective laser melting (SLM) for bone implant applications, Acta Mater. 158 (2018) 354.
[30] R. Wauthle, et al., Additively manufactured porous tantalum implants, Acta Biomater. 14 (2015) 217.
[31] I. Maskery, et al., A mechanical property evaluation of graded density Al-Si10-Mg lattice structures manufactured by selective laser melting, Mater. Sci. Eng. A 670 (2016) 264.
[32] S. Ma, et al., Mechanical behaviours and mass transport properties of bone-mimicking scaffolds consisted of gyroid structures manufactured using selective laser melting, J. Mech. Behav. Biomed. Mater. 93 (2019) 158.
[33] M. Elahinia, et al., Fabrication of NiTi through additive manufacturing: A review, Prog. Mater. Sci. 83 (2016) 630.
[34] C. Tan, et al., Additive manufacturing of bio-inspired multi-scale hierarchically strengthened lattice structures, Int. J. Mach. Tools Manuf. 167 (2021) 103764.
[35] M. Kas, O. Yilmaz, Radially graded porous structure design for laser powder bed fusion additive manufacturing of Ti-6Al-4V alloy, J. Mater. Process. Technol. 296 (2021) 117186.
[36] L.J. Gibson, M.F. Ashby, Cellular Solids Structure and Properties, Cambridge University Press, Cambridge: New York, 1997.
[37] S.L. Sing, et al., Perspectives of using machine learning in laser powder bed fusion for metal additive manufacturing, Virtual Phys. Prototyp. 16 (3) (2021) 372.
[38] Y. Qin, et al., Automatic determination of part build orientation for laser powder bed fusion, Virtual Phys. Prototyp. 16 (1) (2020) 29.
[39] L. Yang, et al., Mechanical response of a triply periodic minimal surface cellular structures manufactured by selective laser melting, Int. J. Mech. Sci. 148 (2018) 149.
[40] X. Cao, et al., Mechanical properties of an improved 3D-printed rhombic dodecahedron stainless steel lattice structure of variable cross section, Int. J. Mech. Sci. 145 (2018) 53.
[41] O. Al-Ketan, et al., Topology-mechanical property relationship of 3D printed strut, skeletal, and sheet based periodic metallic cellular materials, Addit. Manuf. 19 (2018) 167.
[42] L. Dong, Mechanical response of Ti–6Al–4V hierarchical architected metamaterials, Acta Mater. 175 (2019) 90.
[43] L. Dong, Mechanical responses of Ti-6Al-4V cuboctahedral truss lattice structures, Compos. Struct. 235 (2020) 111815.
[44] L. Dong, et al., Mechanical response of Ti–6Al–4V octet-truss lattice structures, Int. J. Solids Struct. 60-61 (2015) 107.
[45] L. Dong, H. Wadley, Mechanical properties of carbon fiber composite octet-truss lattice structures, Compos. Sci. Technol. 119 (2015) 26.
[46] S.C. Han, et al., A New Type of Low Density Material: Shellular, Adv. Mater. 27 (37) (2015) 5506.
[47] X. Zheng, et al., Ultralight, ultrastiff mechanical metamaterials, Science 344 (6190) (2014) 1373.
[48] A. Torrents, et al., Characterization of nickel-based microlattice materials with structural hierarchy from the nanometer to the millimeter scale, Acta Mater. 60 (8) (2012) 3511.
[49] V.S. Deshpande, et al., Effective properties of the octet-truss lattice material, J. Mech. Phys. Solids 49 (2001) 1747.